

# INTERCOMPARISON OF ENERGY FLUX MODELS USING ASTER IMAGERY AT THE SPARC 2004 SITE (BARRAX, SPAIN)

W.J. Timmermans<sup>(1)</sup>, J. van der Kwast<sup>(2)</sup>, A.S.M. Gieske<sup>(1)</sup>, Z. Su<sup>(1)</sup>, A. Olioso<sup>(3)</sup>, L. Jia<sup>(4)</sup>, J. Elbers<sup>(4)</sup>

<sup>(1)</sup>International Institute for Geo-Information Science and Earth Observation (ITC), PO Box 6, 7500 AA Enschede, The Netherlands, E-mail: timmermans@itc.nl

<sup>(2)</sup>Utrecht University, P.O. Box 80115, 3508 TC Utrecht, The Netherlands,

<sup>(3)</sup>INRA, Unité Sol, Climat et Environnement, 84914 Avignon Cédex 9, France

<sup>(4)</sup>ALTEERRA, Wageningen University and Research Centre, P.O. Box 47, 6700 AA, Wageningen, The Netherlands

## ABSTRACT

A comparison of output from three remote sensing based SVAT models is made over the SPARC2004 site in Barrax, Spain. Use is made of ASTER data obtained on the 18<sup>th</sup> of July 2004, overpass 11.008 GMT. Validation versus ground measurements showed reasonable to good results, where errors were generally within measurement accuracy. All three models reflected measured trends in net radiation, soil and sensible heat fluxes; no ground validation of latent heat flux was used.

Inter-comparison of the three models learned that both net radiation and soil heat flux predictions show similar spatial variation, also here differences between the models were nearly negligible. Sensible heat flux output differed mainly between the two-source (TSEB) and the single-source (SEBS and SEBAL) schemes and could be primarily attributed to differences in surface roughness parameterization.

## 1. INTRODUCTION

The estimation of surface energy fluxes can be represented by the balance of available energy against turbulent fluxes:

$$R_N - G = H + LE \quad (1)$$

Where  $R_N$  is net radiation and  $G$  is conducted soil heat and  $H$  and  $LE$  represent the turbulent sensible and latent heat fluxes. A reliable estimation of the partitioning of available energy between sensible and latent heat is of prime interest to the fields of meteorology, hydrology and agronomy. Ample examples range from General Circulation Models (GCM's) for weather prediction and climate change, to water losses in threatened eco-systems, as well as the

determination of crop water stress or vegetation productivity in irrigation systems.

The model parameterization of the interaction between a land surface and the atmosphere is known as a soil-vegetation-atmosphere transfer scheme (SVAT). Numerous SVAT schemes have been developed in recent years with varying complexity. For homogeneous land cover, a single source model is suitable. For more complex canopies, dual source models seem more appropriate. Dual source models have two sets of resistances across which individual, local, single source models are applied and possibly an in-canopy point where such resistances meet, to allow interaction between the soil and vegetation component. A single aerodynamic resistance then connects the combined canopy with the atmosphere. A single source model uses only one resistance and assumes that all the surfaces can be represented by one effective temperature and humidity value.

Although two-source models have a greater physical realism, and as such should reflect the surface energy distribution with greater accuracy than a single source approach, they also require more ancillary data. Moreover, in spite of the simplification of reality in a single source model, many authors have found, after appropriate tuning of the model parameters, that it describes the overall surface energy balance satisfactorily [1], [2], [3]. A simple but correctly calibrated single source model might well perform better than an ill-parameterized dual source model [4]. Therefore, often the simpler single-source schemes are utilized for operational monitoring and forecasting.

Validation of remote sensing based flux estimates are usually performed with a limited number of tower-based flux measurements, supported by some kind of footprint modeling [5]. Little is known, however, about the reliability over the entire landscape. This aspect is of particular interest over a-typical and heterogeneous landcover types, since flux towers are typically situated at homogeneous sites.

To start understanding the differences among various remote sensing based SVAT models, a comparison is made here between surface energy fluxes estimated by three different models. A validation versus ground measurements is performed as well as a spatial inter-comparison. The dataset used here is collected during the SPARC2004 field-campaign, described in more detail in [6]. The objective of the current study is to assess whether the physical simplifications made in the single source models would lead to erroneous predictions, under which circumstances they are likely to occur, and as how to adjust for them.

## 2. ENERGY FLUX MODELING

The modeling schemes used here are SEBAL developed by [7], the SEBS scheme by [8] and the TSEB model, as described by [9].

### 2.1 SEBAL

SEBAL is a one-layer approach that computes surface energy fluxes almost without ancillary data, making it potentially useful for operational monitoring, especially over remote areas. Its main characteristic is its ability to retrieve windspeed and air temperature using the information contained in the spatial variability of the convective fluxes. These are linked to the hydrological contrast of the study area, which is a pre-requisite for the scheme. The model does not need ancillary data, other than first order estimates of wind speed and air temperature, and requires as input maps of kinetic temperature, VIS and NIR reflectance, and incoming solar radiation. Computations are performed using both semi-empirical relations and simplifications of energy balance formulation over dry (zero latent heat flux assumed) and wet (zero sensible heat flux assumed) areas. The surface temperature versus albedo and surface temperature versus NDVI scatterplots are used both to verify the existence of as well as allocate the wet and dry areas.

Rn is computed as the algebraic sum of the shortwave and longwave radiation components, using incoming solar radiation, a first order estimate of air temperature to estimate down-welling longwave radiation, albedo, broadband emissivity and surface radiometric temperature. G is expressed as a semi-empirical fraction of Rn, taking into consideration the effects of surface heating, soil moisture and intercepted solar radiation. The sensible heat flux is computed in steps from flux inversion at dry non-evaporating land units and at wet surface types. At first the surface roughness characteristics are determined using vegetation indices. Then local scale friction velocity is determined from the logarithmic wind profile using wind speed measurements at observation height and calculated

wind speed at blending height. At last air temperature is calculated assuming a linear relation to surface temperature, the coefficients of the relation being calibrated from inverting the sensible heat flux expression over dry and wet areas. The latent heat flux is computed as the residual of the energy balance.

### 2.2 SEBS

SEBS was developed for the estimation of atmospheric turbulent fluxes and surface evaporative fraction (EF) using remote sensing data. In the present set-up, SEBS requires as inputs three sets of information. The first set consists of albedo, temperature, fractional vegetation coverage and leaf area index (when such information is not explicitly available, the normalised difference vegetation index (NDVI) is used as a surrogate), and the height of the vegetation (or roughness height). These inputs can be derived from remote sensing data in conjunction with other information on the land surface. The second set includes the reference or planetary boundary layer (PBL) height, at which pressure, temperature, humidity, and wind speed are available. The reference height is the measurement height for point applications and the height of the planetary boundary for regional applications. This data set can also exist of variables estimated by a large-scale meteorological model. The third data set includes downward long wave radiation, and downward solar radiation which can be either direct measurements, model output or parameterizations.

In order to determine the relative evaporation, use is made of the energy balance considerations at limiting cases. Under the dry-limit, i.e. the latent heat (or the evaporation) becomes zero due to the limitation of the soil moisture, the sensible heat flux is at its maximum value. Under the wet-limit, where the evaporation takes place at maximum rate, i.e. the evaporation is only limited by the available energy under the given surface and atmospheric conditions, the sensible heat flux takes its minimum value. The relative evaporation then can be evaluated as the ratio of the actual to the maximum evaporation rate. The actual sensible heat flux  $H$  is determined with the bulk atmospheric similarity approach and is constrained in the range set by the sensible heat flux at the wet limit  $H_{wet}$ , and that at the dry limit  $H_{dry}$ .  $H_{dry}$  is obtained by assuming zero evaporation and  $H_{wet}$  can be derived by a combination equation following [10] similar to the Penman–Monteith combination equation with the assumption of a completely wet situation.

### 2.3 TSEB

The main characteristic of TSEB is to use a two-source approach that discriminates the soil and vegetation component, aiming at a more physical description of heterogeneous surfaces when dealing with radiative and aerodynamic properties. The model requires as input information maps of kinetic temperature, Normalized Difference Vegetation Index (NDVI), land use, incoming solar and thermal radiation, as well as micrometeorological measurements of air temperature, humidity, air pressure and wind speed. As suggested by [11], fractional vegetation cover is computed using a scaled NDVI. Leaf Area Index (LAI) is deduced from the fractional vegetation cover using a logarithmic function. Vegetation height is deduced from the land use map along with a look up table calibrated from field observations. Radiative properties of the canopy are computed using the divergence of net radiation method, [12], along with radiative properties of soil and vegetation that are set to nominal values. Roughness length for momentum is set to 1/8<sup>th</sup> of the vegetation height. Radiative transfer inside canopy is modeled considering the multiple scattering between the soil and vegetation. R<sub>n</sub>, H and LE are computed for both soil and vegetation. G is computed as a fraction of soil net radiation, the fraction being set to a nominal value. Using a two-source remote sensing approach along with single direction observations such as was the case for the ASTER imagery, requires adding some assumptions to compute soil and vegetation temperatures. This is performed deducing the vegetation latent heat flux from vegetation net radiation using the Priestly-Taylor (PT) relation. Further, composite radiative temperature is expressed as a weighted sum of vegetation and soil temperatures, the weights being the fractional vegetation cover and its complementary to unity, respectively. Finally, vegetation sensible heat flux and soil latent heat flux are computed as the residues of the vegetation and soil energy balance respectively.

However, the PT relation only provides an initial calculation of the latent heat flux for soil, and it can be overridden if the temperature difference between the soil - canopy system and the atmosphere is large, causing erroneous flux estimates. If the estimated radiometric temperature is less than the measured one, then the PT approximation will tend to overestimate the canopy transpiration rate because the water supply in the root zone is inadequate. Therefore, an iteration procedure will compute latent heat fluxes for vegetation below estimates given by the PT estimation until values of canopy and soil temperature agree with the measured radiometric temperature, [13].

### 2.4 Model similarities

All three models provide estimates of energy fluxes by solving Eq. 1. This is done by first estimating the net radiation, following:

$$R_N = (1 - \rho_0) \cdot R_s^{\downarrow} + \varepsilon_0 \cdot \varepsilon_a \cdot \sigma \cdot T_a^4 - \varepsilon_0 \cdot \sigma \cdot T_0^4 \quad (2)$$

where “R” stands for radiation, and the subscripts “N” and “S”, refer to net and shortwave. The greek letters “ρ”, “ε”, and “σ” represent albedo, emissivity and the Stefan-Boltzmann constant, respectively. The subscripts “0” and “a” refer to surface and atmospheric level. Only a slight difference exists in estimating the apparent emissivity of the atmosphere, ε<sub>a</sub>, where a physically based expression [14] is used in TSEB and a semi-empirical approach in SEBAL and SEBS. As a consequence, differences in net radiation estimation are relatively small between the schemes.

The soil heat flux is generally estimated as a ratio to net radiation. The main difference is that in TSEB and SEBS an attempt is made to model the soil heat flux as a fraction of the soil component of net radiation using the fractional vegetation cover [15], whereas SEBAL uses a semi-empirical approach to estimate net radiation extinction in the canopy, as a function of the normalized difference vegetation index:

$$\Gamma = T_0 / \rho_0 \cdot (a_1 c_1 \rho_0 + a_2 \cdot (c_1 \rho_0)^2) \cdot (1 - b_1 NDVI^4) \quad (3)$$

where coefficient c<sub>1</sub> is a parameter used to convert instantaneous albedo values to daily averages, usually taken equal to 1.1. The coefficients a<sub>1</sub>, a<sub>2</sub> and b<sub>1</sub> stem from the original SEBAL formulation and should be locally calibrated if possible. However, since SEBAL was developed in this particular study area, the original values, 0.0032, 0.0062 and 0.978 respectively, are taken. Although nominal values are used in the TSEB and SEBS approach, results for soil heat flux estimation do not differ greatly with those of SEBAL.

### 2.5 Model differences

Apart from the conceptual difference between one- and two-source models, there are some other differences in how land-atmosphere exchanges are parameterized. The main differences are related to aerodynamic and thermal dynamic roughness parameterization and, to a lesser extent, the atmospheric stability. All of them however, are related to the determination of the sensible heat flux, commonly described by a physically based resistance network, following:

$$H = \frac{\rho_a \cdot C_p}{r_{ah}} \cdot (\theta_0 - \theta_a) \quad (4)$$

where  $\rho_a$  is the air density,  $C_p$  the specific heat of air at constant pressure,  $\theta_0$  represents potential temperature at the surface and  $\theta_a$  is the potential temperature of the overlying air at reference height  $z$ , and  $r_{ah}$  is the aerodynamic resistance to heat, given by:

$$r_{ah} = \frac{\left[ \ln\left(\frac{z-d_0}{z_{0M}}\right) - \psi_M(z, L_{MO}) \right] \cdot \left[ \ln\left(\frac{z-d_0}{z_{0H}}\right) - \psi_H(z, L_{MO}) \right]}{k^2 \cdot u} \quad (5)$$

where  $d_0$  is the zero plane displacement height,  $z_{0M}$  the roughness height for momentum transfer,  $z_{0H}$  the scalar roughness height for heat transfer,  $k$  the Von Karman constant,  $u$  the windspeed at height  $z$ ,  $\psi_M$  and  $\psi_H$  the stability correction functions for momentum and sensible heat transfer respectively, and  $L_{MO}$  is the Monin-Obhukov length defined as:

$$L_{MO} = -\frac{\rho_a \cdot C_p \cdot u_*^3 \theta_v}{k \cdot g \cdot H} \quad (6)$$

where  $g$  is the acceleration due to gravity and  $\theta_v$  the potential virtual temperature near the surface.

Where SEBAL and SEBS utilize a single surface potential temperature to solve the set of equations (5) – (7), the TSEB scheme considers the contributions from the soil and canopy separately and requires a few additional parameters to solve for sensible heat. In the version applied here, the sensible heat flux,  $H$ , is expressed as the sum of the contribution from the soil,  $H_s$ , and from the canopy,  $H_c$ , following:

$$H = H_s + H_c = \rho_a \cdot C_p \cdot \left[ \frac{(\theta_c - \theta_a)}{r_{ah}} + \frac{(\theta_s - \theta_a)}{r_{ah} + r_s} \right] \quad (7)$$

where subscripts  $c$  and  $s$  refer to canopy and soil respectively. The resistance to aerodynamic heat transfer,  $r_{ah}$ , is defined in Eq. (5), whereas the resistance to heat flow in the boundary layer immediately above the soil surface,  $r_s$ , is taken from [16]. They derived semi-empirical relations linking  $r_s$  to canopy leaf-width,  $w$ , and windspeed just above the surface.

Whereas the SEBAL and SEBS try to parameterize the roughness lengths by using hardly any ancillary data, TSEB takes these roughness characteristics from a landcover map using nominal values, see Table 1.

Another difference between the schemes compared here is the functions that are used for calculating atmospheric stability. Although it is believed that these do not create significant deviations between the models, they are mentioned here for the sake of completeness.

The version of TSEB used here [9] and SEBAL utilize the Monin-Obhukov Similarity (MOS) functions given by [14] for both unstable and stable conditions. SEBS on the other hand uses the criterion of [17] to determine if MOS or Bulk Atmospheric Boundary Layer Similarity (BAS) scaling is appropriate for a

given situation. For unstable conditions SEBS uses the expressions proposed by [18] for MOS scaling and the functions suggested by [14] for BAS scaling.

Summarizing, the models use only slightly different approaches to arrive at net radiation and soil heat flux, but these approaches are not characteristic for the models, and are even inter-changeable. Although the method for modeling the sensible heat flux is similar in the sense of a resistance network approach, the approaches are different in nature as seen from the source approach. Therefore, focus in this inter-comparison was put on the sensible heat flux. Furthermore, because in the SEBAL scheme the latent heat flux is calculated as a rest-term, error accumulation occurs in this parameter, which makes it less suitable for comparison. In addition, the latent heat flux was only measured at one specific site, providing very limited validation data.

### 3. DATA DESCRIPTION

ASTER's excellent capabilities for surface energy flux mapping [19], ASTER has 15m. resolution in 3 visible-near infrared bands and 90m. resolution in 5 thermal infrared bands, are used over the Barrax site for the 18<sup>th</sup> of July 2004. Local overpass time was 11.008 GMT. Required remotely sensed input for the schemes compared here are broadband surface albedo, horizontal and vertical vegetation density (fractional cover and LAI respectively), NDVI and surface temperature. Broadband surface albedo is derived from 6 shortwave channels following [20], vegetation density is retrieved from NDVI using 2 VNIR bands and a method described by [11], whereas surface temperature is retrieved from a temperature-emissivity separation (TES) algorithm [21] using all five TIR bands.

The ground-based data used in this study are collected on the 18<sup>th</sup> of July 2004, during the SPARC2004 field-campaign at Barrax, Spain, Figure 1. Apart from the standard meteorological measurements they consisted of radiation and flux tower observations, measuring the incoming and outgoing shortwave and longwave radiation as well as soil and sensible heat fluxes at different sites. Latent heat flux was only measured in one site during this particular day and is therefore not used here.

Measurements were performed over typical land-cover units, comprising of a forest nursery (F), a wheat stubble field (CW1), vineyard (V), a sunflower field (SF1) and a corn fields (C2). Details of the measurements are provided in [6].

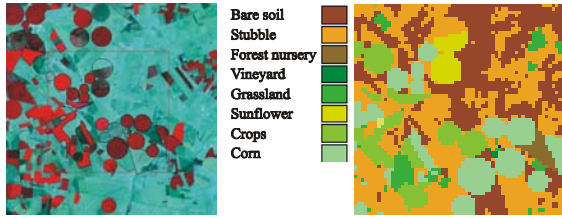


**Figure 1.** ASTER image overlay with landuse interpretation from the SPARC2004 landuse database (left). On the right side the landuse map at 90 meter resolution is shown.

Apart from the remote sensing data and meteorological information, the TSEB model needs surface parameters information for typical land-cover units. They comprise of canopy height,  $h_c$ , surface roughness for momentum transport,  $z_{0M}$ , zero-plane displacement height,  $d_0$ , and leaf-width,  $w$ , which are tabulated in Table 1. A note has to be made with regard to the surface roughness values as given for the forest nursery and the vineyard. Due to the structure of these orchards, i.e. row orientation, the roughness value may vary considerably depending on wind direction, a topic for future research.

**Table 1.** Surface parameters for the different landcover types.

Landcover	$h_c$	$z_{0M}$	$d_0$	$w$
Bare soil	-	0.005	-	-
Stubble	0.15	0.015	0.10	0.001
Forest nursery	0.35	0.06*	0.23	0.001
Vineyard	1.25	0.15*	0.83	0.050
Grassland	0.02	0.0025	0.013	0.005
Sunflower	1.0	0.125	0.65	0.05
Irrigated crops	0.25	0.03125	0.163	0.02
Corn	2.0	0.25	1.3	0.05

The landcover map, as shown on the right side in Figure 1, is derived from a combination of the SPARC2004 landuse database and a supervised classification using the ASTER 15m resolution imagery of the 18<sup>th</sup> of July 2004.

#### 4. MODEL VALIDATION AT SPARC 2004

Validation of model output is performed by comparison with tower-based flux observations [6]. Using the remote sensing derived model output and footprint weighted, following [22], ground-based flux components are compared for 5 sites. To compare and contrast spatially distributed output of the schemes, the sites were selected such that the widest range in turbulent fluxes that might exist in the area were covered. Example output is shown in Figure 2, where TSEB (left) and SEBS (right) results for sensible heat flux are displayed.

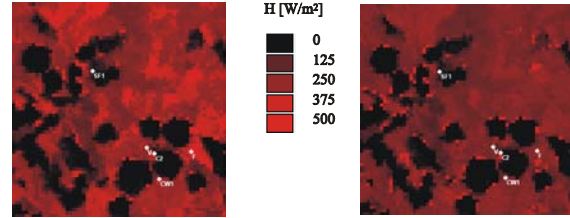


**Figure 2.** Sensible heat fluxes ( $H$ ) from TSEB (left) and SEBS (right) over the 18 July 2004 Barrax SPARC study area.

The results for all three models versus ground observations are shown in Fig.3, where modeled output is shown on the y-axis and observations on the x-axis. A diamond represents TSEB, a triangle is SEBS and a square shows the SEBAL results.

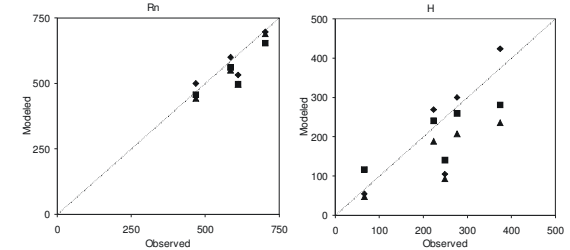


**Figure 3.** Validation results for all three models showing results for net radiation (left) and sensible heat flux (right).

Net radiation estimates do not differ greatly with the observations from either model, although all three models show a slight under-estimation over the vineyard. This may be due to the field of view of the net radiometer, which included a minor part of a dirt road next to the vineyard, resulting in slightly higher reflection values and thus lower net radiation values. Soil heat fluxes, not shown, showed similar good responses, although all three models yielded slightly under-estimated values over lowest vegetation covers.

With regard to the sensible heat fluxes, all three models perform reasonably well for all land-cover types, especially considering the uncertainty in  $H$  tower measurements. A minor exception has to be made with respect to the higher sensible heat fluxes for both SEBAL and SEBS, which show under-estimated values with respect to ground observations up to 100 and 140  $W/m^2$  respectively; a common observation when comparing one- and two-source models over sparsely vegetated areas [1, 23].

All three schemes follow the measured trend, however, a notable exception is seen for the C2 site. As may be clear from Figure 2, this site was positioned right at the edge of the corn field C2, in order to examine the wind-directional influence. However, due to the mixed nature of the pixels contributing to the footprint of the C2 measurement, results were hard to interpret.

This is also the explanation for the spikes in the sensible heat flux output as seen at the edge of different

landuse types, Figure 2, notably at transitions between wet, irrigated crops and dry bare soil or wheat stubble fields. Especially in the SEBS and SEBAL schemes this effect was very pronounced, due to the use of semi-empirical relations, who assume homogeneous, pure pixels. These pixels should be excluded from the analysis at this spatial resolution (90m). Additional analysis at higher resolution, such as the AHS imagery, is needed at these transitions. Future work is scheduled to examine these edge effects and footprint influence.

## 5. MODEL INTERCOMPARISON

Since remote sensing methods claim to be useful in providing spatially distributed fluxes, a comparison of model output over the entire study area is of major interest. A proper model result in the ground observation points does not necessarily imply a good over-all fit. Usually limited ground observation points are available and calibration, or fine-tuning, is performed to obtain the best fit possible. Moreover, observation points are usually put in positions that represent homogenous areas with well-defined, or even measured, surface characteristics. These points typically do not represent extreme conditions, which are of special interest. Therefore, a closer look is taken at spatial differences in model output.

The results from the ASTER-based inter-comparison are reflected in two-dimensional scatter-plots on a pixel-by-pixel basis, Fig. 4. Because the output for SEBAL and SEBS were rather similar, only the scatter-plots between TSEB and SEBS are shown here. All four components of the energy balance, Eq. 1, are shown in Fig. 4, where the TSEB results are plotted on the x-axis and SEBS results on the y-axis. Please note that differences in the Rn and G case are exaggerated with respect to the turbulent fluxes H and LE, because the axis scales are not identical for the four plots.

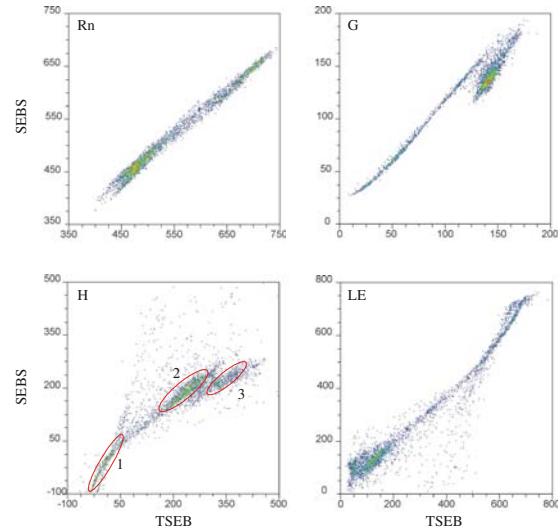


**Figure 4.** Two-dimensional scatterplots of TSEB (x-axis) versus SEBS (y-axis) model outputs. The upper left shows net radiation results, clockwise followed by soil heat, latent and sensible heat flux output.

The plots show how model estimates for the different components relate to each other by showing the frequency distribution over the entire study area. A pseudo color representation is chosen, such that red represents high and blue represents low occurrence.

Net radiation and soil heat flux, as in the ground validation, show very similar results. Especially the net radiation output is almost identical, which is not surprising, since the main difference is the treatment of apparent atmospheric emissivity, yielding a more or less constant off-set. Soil heat flux shows a minor scatter, but differences are generally less than  $35 \text{ W/m}^2$ . However, a note has to be made here, that spatial variation is less for the SEBAL output as compared to TSEB and SEBS. This is because both TSEB and SEBS utilize the fractional vegetation cover for determining the part of net radiation that goes to the soil, where SEBAL uses a semi-empirical relation, Eq. (3), developed in this particular area. Due to the nature of Eq. (3) an off-set is seen at low soil heat flux rates for SEBAL with respect to the other two schemes.

As stated before, the turbulent fluxes are strongly correlated; high sensible heat flux implies low latent heat flux. In parts the latent heat flux is even calculated as a rest-term, therefore the focus here is on the sensible heat only.

It is already noticed in section 4, that over the drier regions sensible heat flux output was higher for TSEB than for the other two schemes. This is also reflected in the lower left scatterplot of Fig. 4. Although the majority of the plot approaches the 45 degree line, it is also clear that pixels appear in clusters. Analysis learnt that these clusters are related to land use classes, a

phenomenon discussed in somewhat more detail in section 6.

## 6. DISCUSSION

Validation versus ground observation and also model inter-comparison learnt that all three models respond similarly to ASTER based inputs of albedo, vegetation characteristics and temperature over the Barrax site. Patterns in all four flux components are similar for the three models, although over drier areas the TSEB scheme shows higher values for sensible heat.

As stated above, model output for sensible heat fluxes differed mainly with land-cover type. This is not surprising, because of the difference in parameterization of aerodynamic and thermal dynamic roughness, see section 2.5.

**Table 2.** Surface roughness for momentum, averaged per land-cover type, between brackets the standard deviation is shown.

Landcover	TSEB	SEBS	SEBAL
Bare soil	0.005	0.019 (0.024)	0.012 (0.013)
Stubble	0.015	0.036 (0.054)	0.020 (0.032)
Forest nursery	0.06	0.065 (0.092)	0.035 (0.055)
Vineyard	0.15	0.125 (0.163)	0.073 (0.109)
Grassland	0.0025	0.166 (0.127)	0.088 (0.091)
Sunflower	0.125	0.162 (0.064)	0.074 (0.034)
Irrigated crops	0.03125	0.277 (0.181)	0.180 (0.134)
Corn	0.25	0.342 (0.115)	0.211 (0.084)

TSEB takes the aerodynamic roughness directly from a land-cover map, whereas the other two schemes have parameterized the surface roughness for momentum from the remote sensing data itself, see Table 2. The three main clusters that are seen in the lower left plot of Fig.4 are related to irrigated fields (1), bare soil (2) and wheat stubble fields (3).

What is surprising though, is that SEBS and SEBAL output for the drier areas (bare soil and stubble mainly) sensible heat is somewhat lower than TSEB output for these regions. Especially for the drier areas the SEBAL and SEBS values for  $z_{0M}$  are higher than those in TSEB. Generally, when increasing surface roughness, aerodynamic resistances decrease which in turn results in higher sensible heat fluxes. Therefore some compensation effect must take place at some point.

It is believed that the most plausible cause is the parameterization of the near surface potential temperature difference, because the other major factor in estimating sensible heat flux is the difference between potential temperature at the surface and potential temperature of the overlying air. Therefore a more thorough investigation of how the different models treat this near surface temperature difference is needed, which is under way.

## 7. REFERENCES

1. Kustas, W.P., et al., Single- and dual-source modeling of surface energy fluxes with radiometric surface temperature. *Journal of Applied Meteorology*, 1996. 35(1): p. 110-121.
2. Troufleau, D., et al., Sensible heat flux and radiometric surface temperature over sparse Sahelian vegetation. I. An experimental analysis of the kB-1 parameter. *Journal of Hydrology*, 1997. 188-189: p. 815-838.
3. Bastiaanssen, W.G.M., et al., A remote sensing surface energy balance algorithm for land (SEBAL): 2. Validation. *Journal of Hydrology*, 1998. 212-213: p. 213-229.
4. Kustas, W.P., Estimates of evapotranspiration within a one-and two-layer model of heat transfer over partial vegetation cover. *Journal of Applied Meteorology*, 1990. 29: p. 704-715.
5. Horst, T.W. and J.C. Weil, Footprint estimation for scalar flux measurements in the atmospheric surface layer. *Boundary-Layer Meteorology*, 1992. 59: p. 279-296.
6. Su, Z., et al., In-situ measurements of land-atmosphere exchanges of water, energy and carbon dioxide in space and time over the heterogeneous BARRAX site during SPARC2004. *ESA Proceedings WPP-250, SPARC Final Workshop, ITC Enschede, 4-5 July 2005, The Netherlands*, 2005.
7. Bastiaanssen, W.G.M., et al., A remote sensing surface energy balance algorithm for land (SEBAL): 1. Formulation. *Journal of Hydrology*, 1998. 212-213: p. 198-212.
8. Su, Z., The Surface Energy Balance System (SEBS) for estimation of turbulent heat fluxes. *Hydrology and Earth System Sciences*, 2002. 6(1): p. 85-99.
9. Norman, J.M., W.P. Kustas, and K.S. Humes, A two-source approach for estimating soil and vegetation energy fluxes in observations of directional radiometric surface temperature. *Agricultural and Forest Meteorology*, 1995. 77: p. 263-293.
10. Menenti, M. and B.J. Choudhury, Parameterization of land surface evaporation by means of location dependant potential evaporation and surface temperature range. *Exchange Processes at the Land surface for a range of space and time scales*, 1993. Proceedings of the Yokohama Symposium (IAHS Publ. no 212).
11. Choudhury, B.J., et al., Relations between evaporation coefficients and vegetation

- indices studied by model simulations. *Remote Sensing Environment*, 1994. 50: p. 1-17.
12. Campbell, G.S. and J.M. Norman, An introduction to Environmental Biophysics. *Springer, New York*, 1998. ISBN 0-387-94937-2: p. 286 pp.
  13. Kustas, W.P. and J.M. Norman, Evaluating the effects of subpixel heterogeneity on pixel average fluxes. *Remote Sensing Environment*, 2000. 74: p. 327-342.
  14. Brutsaert, W., Evaporation into the atmosphere. *Reidel, Dordrecht, The Netherlands*, 1982: p. 299.
  15. Kustas, W.P. and C.S.T. Daughtry, Estimation of the soil heat flux/net radiation ratio from spectral data. *Agricultural and Forest Meteorology*, 1990. 49: p. 205-223.
  16. Sauer, T.J., et al., Measurement of heat and vapor transfer coefficients at the soil surface beneath a maize canopy using source plates. *Agricultural and Forest Meteorology*, 1995. 75: p. 161-189.
  17. Brutsaert, W., Aspects of bulk atmospheric boundary similarity under free-convective conditions. *Reviews of Geophysics*, 1999. 37: p. 439-451.
  18. Beljaars, A.C.M. and A.A.M. Holtslag, Flux parameterization over land surfaces for atmospheric models. *Journal of Applied Meteorology*, 1991. 30: p. 327-341.
  19. French, A.N., et al., Surface energy fluxes with the Advanced Spaceborne Thermal Emission and Reflection radiometer (ASTER) at the Iowa 2000 SMACEX site (USA). *Remote Sensing of Environment*, 2005. In press.
  20. Liang, S., Narrowband to broadband conversions of land surface albedo: I. Algorithms. *Remote Sensing Environment*, 2000. 76: p. 213-238.
  21. Gillespie, A., et al., A temperature and emissivity separation algorithm for Advanced Spaceborne Thermal Emission and Reflection Radiometer (ASTER) images. *IEEE Transactions on geoscience and remote sensing*, 1998. 36(4): p. 1113-1126.
  22. Soegaard, H., et al., Carbon dioxide exchange over agricultural landscape using eddy correlation and footprint modelling. *Agricultural and Forest Meteorology*, 2003. 114: p. 153-173.
  23. Huntingford, C., A. Verhoef, and H. Stewart, Dual versus single source models for estimating surface temperature of African savannah. *Hydrology and Earth System Sciences*, 2000. 4(1): p. 185-191.